Nucl Eng Technol 47 (2015) 746–755

Available online at www.sciencedirect.com

ScienceDirect

journal homepage: http://www.journals.elsevier.com/nuclear-engineering-and-technology/

Original Article

THE EFFECT OF HYDROGEN AND OXYGEN CONTENTS ON HYDRIDE REORIENTATIONS OF ZIRCONIUM ALLOY CLADDING TUBES

*HYUN-JIN CHA, KI-NAM JANG, JI-HYEONG AN, and KYU-TAE KIM**

Dongguk University, College of Energy and Environment, 707 Seokjang-Dong, Gyeongju, Gyeongbuk, 780-714, Republic of Korea

ARTICLE INFO

Article history:
Received 4 April 2015
Received in revised form
26 June 2015
Accepted 26 June 2015
Available online 11 August 2015

Keywords:
Hydride precipitation
Hydrogen solubility
Mechanical property
Zirconium alloy

ABSTRACT

To investigate the effect of hydrogen and oxygen contents on hydride reorientations during cool-down processes, zirconium–niobium cladding tube specimens were hydrogen-charged before some specimens were oxidized, resulting in 250 ppm and 500 ppm hydrogen-charged specimens containing no oxide and an oxide thickness of 3.8 μm at each surface. The nonoxidized and oxidized hydrogen-charged specimens were heated up to 400°C and then cooled down to room temperature at cooling rates of 0.3°C/min and 8.0°C/min under a tensile hoop stress of 150 MPa. The lower hydrogen contents and the slower cooling rate generated a larger fraction of radial hydrides, a longer radial hydride length, and a lower ultimate tensile strength and plastic elongation. In addition, the oxidized specimens generated a smaller fraction of radial hydrides and a lower ultimate tensile strength and plastic elongation than the nonoxidized specimens. This may be due to: a solubility difference between room temperature and 400°C; an oxygen-induced increase in hydrogen solubility and radial hydride nucleation energy; high temperature residence time during the cool-down; or undissolved circumferential hydrides at 400°C.

1. Introduction

During the interim dry storage of spent nuclear fuel, the fuel rod internal pressure can generate tensile hoop stress on the zirconium alloy cladding tubes that cool down very gradually from various cladding tube peak temperatures of between 200°C and 400°C over several decades. This interim dry storage condition may generate tensile hoop stress-induced hydride reorientation in the radial direction of the cladding tube and reduce the cladding's ductility. The aforementioned stress-induced hydride reorientation behavior in zirconium alloys has been investigated by many researchers [1–12]. Based on these research results, it can be said that the amount of radial hydrides formed during the interim dry storage period may be dependent on hydrogen solubility in the zirconium alloy cladding, heat-up cladding temperatures during the fuel dry

* *Corresponding author.*
E-mail address: ktkim@dongguk.ac.kr (K.-T. Kim).

http://dx.doi.org/10.1016/j.net.2015.06.004
1738-5733/Copyright © 2015, Published by Elsevier Korea LLC on behalf of Korean Nuclear Society.

period, tensile hoop stresses, cool-down rates, hydrogen contents, etc. In addition, it was reported that the formation of radial hydrides in the cladding tubes may be closely related to their fabrication histories, textures, and stress states [13–16].

However, sufficient data on hydride reorientation behaviors during cool-down have not been provided for spent fuel cladding conditions that simulate both oxygen and hydrogen contents as well as neutron irradiation-induced microstructure changes. It is noteworthy that the hydrogen solubility increased with the oxygen-containing Zircaloy-4 materials [17], while it increased in the lower oxygen content range but decreased in the higher oxygen content range [18]. In this study, therefore, the effect of both hydrogen and oxygen contents on the hydride reorientation behaviors, such as radial hydride fractions and lengths, was investigated along with various tensile hoop stresses and cool-down rates.

In general, a temperature limit of 400°C, which is specified for normal and short-term transient conditions during the interim dry storage, will limit cladding hoop stresses and the amount of dissolved hydrogen atoms available to precipitate hydrides during the cool-down [14]. It is generally recognized that the hydrogen content in cladding should be controlled to below 600 ppm-H and the fuel rod internal pressure should be controlled to below the reactor coolant system pressure (15.5 MPa) that may cause a tensile hoop stress of 150 MPa on the cladding tube during the interim dry storage period. It is also reported that the cladding may cool down over several decades by about 100°C per 10 years (2×10^{-5}°C/min) [19]. It is also noted that the zirconium–niobium (Zr-Nb) alloy cladding tubes have been used mostly for pressurized water reactors.

In this study, therefore, stress relieved annealed (SRA) Zr-Nb cladding alloys were employed. The test matrix included two hydrogen contents, one tensile hoop stress and two cooling rates, simulating the spent fuel conditions at the interim dry storage conditions. Firstly, based on the aforementioned allowable maximum hydrogen content of 600 ppm, two hydrogen contents of 250 ppm and 500 ppm in the SRA Zr-Nb tube specimens were used to evaluate the effect of hydrogen content on the hydride orientation behaviors. Secondly, the aforementioned maximum tensile hoop stress of 150 MPa was employed to evaluate the effect of the maximum tensile hoop stress on the hydride reorientation. Lastly, considering the expected slowest cooling rate 2×10^{-5}°C/min during the interim dry storage, two cooling rates of 0.3°C/min and 8.0°C/min were selected to evaluate the effect of cooling rate on the hydride reorientation. The Zr-Nb tube specimens were oxidized to 3.8 μm at their inner and outer surfaces to evaluate the effect of oxidation on the hydride reorientation. The specimens were heated up to 400°C with one heating rate of 3.0°C/min and then remained at that temperature for 2 hours to provide enough time for hydride dissolution prior to cool-down. The specimens were cooled down to room temperature with the respective cooling rates of 0.3°C/min and 8.0°C/min under the tensile hoop stress of 150 MPa.

2. Material and methods

Chemical compositions, texture and dimensions of the Zr-Nb cladding tubes used in the pressurized water reactors are given in Table 1. The Zr-Nb cladding tubes that were cold-pilgered and stress-relieved were supplied by the Korea Nuclear Fuel Company. These cladding tubes were cut into several parts of 100 mm each before the tube surfaces were cleaned with acetic acid. Two parts of the tubes were charged with hydrogen in a vacuum furnace at 400°C containing a mixture gas of hydrogen (150 mmHg) and helium (200 mmHg) to generate a uniform distribution of hydrogen through the tubes [20]. The hydrogen contents of the test specimens were analyzed by the LECO hydrogen analyzer RH600. Various hydrogen contents of the test specimens were generated, including 200 ± 20 ppm, 250 ± 20 ppm, 450 ± 20 ppm, and 500 ± 20 ppm. Only the hydrogen-charged specimens of 200 ppm and 450 ppm were oxidized for ~60 days at 360°C and 17.5MPa in an autoclave under the water atmosphere, resulting in about 3.8 μm at each surface of the test specimens. These oxidized hydrogen-charged specimens were found to contain respective hydrogen concentrations of 250 ± 25 ppm and 500 ± 25 ppm, indicating that hydrogen pickup occurred during the oxidation process in the autoclave. After heating up the oxidized specimens to 400°C and holding them at that temperature for 2 hours, the signal detector (SEM-EDS)–XFlash6 was employed to measure oxygen content in the metal region. Before the oxygen content measurements, the specimens were polished to remove any surface contamination. The oxygen atoms in the metal phase appear to be distributed nearly uniformly. The oxygen content in the metal phase were measured to be 2.0 ± 1.5 w/o (weight percent) for the oxidized specimens.

Fig. 1 shows a schematic configuration of the test specimen and two half-cylinder loading pins that open and strain the test specimen. The test specimens were cut transversely from the cladding tubes to make a width of 5 mm. The diameter of the half-cylinder loading pin is 8.35 mm and the gage length of the test specimens is 2 mm. Special grips were designed and fabricated to fix the loading pins and apply some load on the test specimen. As seen in Fig. 2, the test specimens were heated up to 400°C at 3.0°C/min and remained for 2 hours at that temperature. Then, the oxidized specimens were cooled down with two cooling rates of 0.3°C/min and 8.0°C/min under the tensile hoop stress of 150 MPa. The cooling rate of 0.3°C/

Table 1 – Zirconium alloy cladding tubes used in this work.

Materials	Chemical composition (w/o)	Texture (Kearns number)	Tube dimension (mm)
Zr alloy	Zr-1.0Nb-1.0Sn-0.1Fe-0.12O	f_r (radial) = 0.62 f_t (tangential) = 0.26 f_a (axial) = 0.12	Outer dia. = 9.50 Thickness = 0.57

Fe, iron; Nb, niobium; Sn, tin; w/o, weight percent; Zr, zirconium.

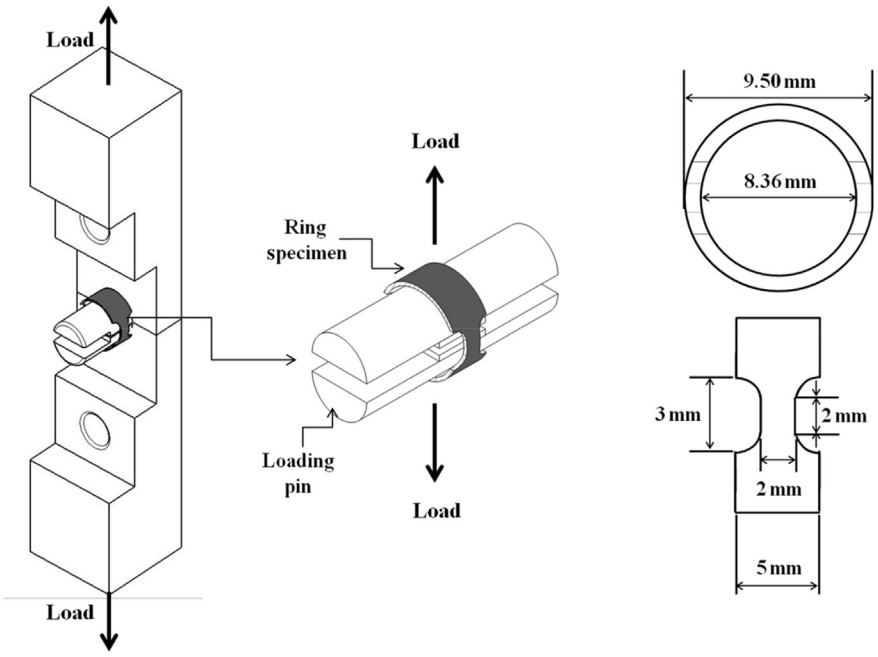

Fig. 1 – Configurations of a ring specimen and jigs/fixtures used in this work.

min represents the average cool-down rate of the gage region of the specimen when the furnace power switch is just off, whereas the cooling rate 8.0°C/min represents the average cool-down rate of the gage region when the specimen is water-quenched. It should be noted that the temperature gradient along the gage length of the specimens was not detectable. Hydride orientation tests were carried out using the KLES 500-S creep tester. After the cool-down tests, tensile tests were conducted at room temperature using an Instron model 3366 mechanical testing machine at a nominal strain rate of 0.001/s (0.12 mm/min) to produce ultimate tensile stresses and plastic elongations. By contrast, to check the reproducibility of the test results, the cooling tests were repeated twice using the same batch of the test specimens.

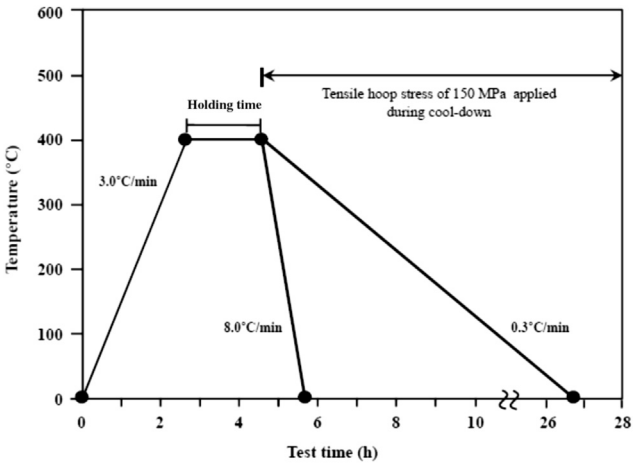

Fig. 2 – Heat-up and cool-down processes used in this work.

Before and after the heat-up and cool-down tests, the gage regions were cut along the axial direction and then the cut sections were examined by an optical microscopy to reveal the fractions of radial and circumferential hydrides and their lengths. The etchant used for metallographic examination was composed of HF, HNO_3, and H_2O in a volume ratio of 10:45:45.

3. Results and discussion

Prior to the heat-up tests, the axially cut sections of the test specimens were examined by scanning electron microscopy to reveal the hydride and oxide configurations of the oxidized 250 ppm-H and 500 ppm-H specimens. Fig. 3 shows that most of the hydrides appear to be oriented in the circumferential direction and the 3.8-μm oxide layers were formed at both inner and outer surfaces. The circumferential hydrides may be closely correlated to their texture [9,14,15]. As shown in Table 1, the Kearns numbers of the Zr-Nb alloy tubes were measured to be 0.62, 0.26, and 0.12 for radial, tangential, and axial basal poles, respectively. Therefore, it may be expected that the radial basal pole will generate the circumferential hydrides, whereas the tangential basal pole will generate the radial hydrides. However, it was found that the specimens charged with hydrogen at 400°C under no stress condition generated the hydrides mostly in the circumferential direction, as shown in Fig. 3, indicating that a certain threshold tensile hoop stress is needed for the radial hydride formation during the cool-down process [2,21–23].

The test specimens were heated up from room temperature (RT) to the peak heat-up temperature of 400°C (see Fig. 2). Then, the test specimens were quenched to room temperature

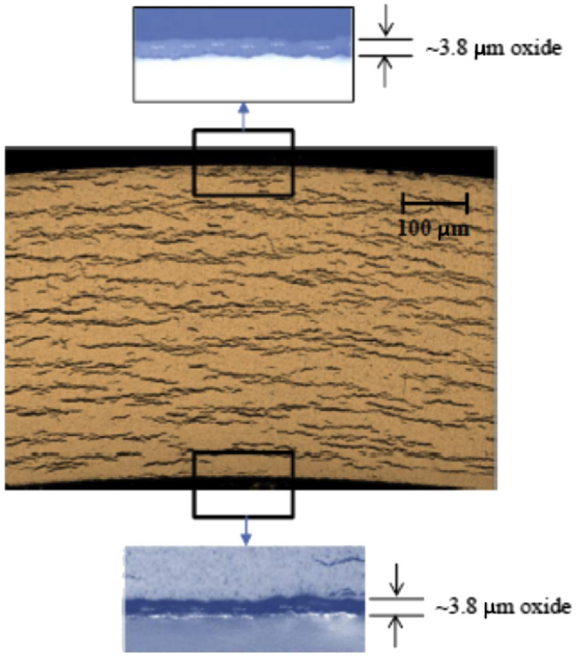

Fig. 3 – An optical micrograph of the 250 ppm-H and 7.6 μm oxidized specimen.

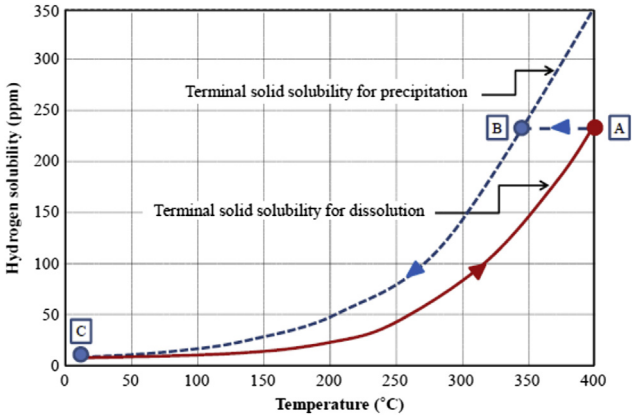

Fig. 5 – Terminal solid solubility of hydrogen in the Zircaloy-4 claddings.

to freeze the hydride distribution at 400°C. The optical micrographs before and after the heat-up are shown in Fig. 4. Comparison of the micrographs between 400°C and RT indicate that most of the hydrides in the 250 ppm-H specimens were dissolved at that heat-up temperature, while about half of the hydrides in the 500 ppm-H specimens were dissolved. This hydride dissolution behavior may be explained by the terminal solid solubility for dissolution [24]. From Fig. 5, it can be seen that the hydrogen solubility for dissolution at 400°C is ~230 ppm, as given in [24], indicating that most of the hydrides in the 250 ppm-H specimens may be dissolved at 400°C, whereas about half of the hydrides in the 500 ppm-H may be dissolved.

Using the respective nonoxidized and oxidized specimens, two kinds of the cool-down tests were performed from 400°C to RT with the cooling rate of 8.0°C/min (water cooling) and 0.3°C/min (furnace cooling) under the tensile hoop stress of 150 MPa, as shown in Fig. 2. The optical micrographs for the nonoxidized and oxidized specimens are shown in Fig. 6. In general, it was found that the radial hydride fraction increases when moving from the outer to the inner surface. This phenomenon may be explained by a cladding tensile hoop stress variation along the cladding diameter. Fig. 7 shows a calculated tensile hoop stress curve when applying an average stress of 150MPa on the cladding, assuming the thick wall cylinder. As mentioned above, a certain threshold tensile hoop stress may be needed for the radial hydride formation during the cool-down process and the radial hydride

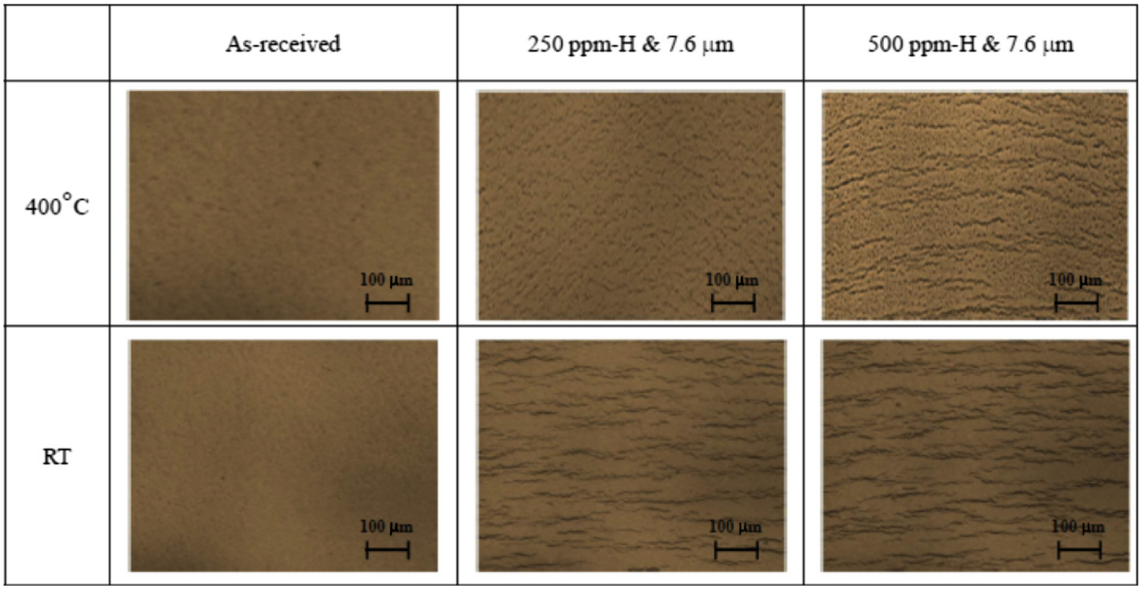

Fig. 4 – Hydrogen content- and oxygen content-dependent optical micrographs at room temperature and 400°C.

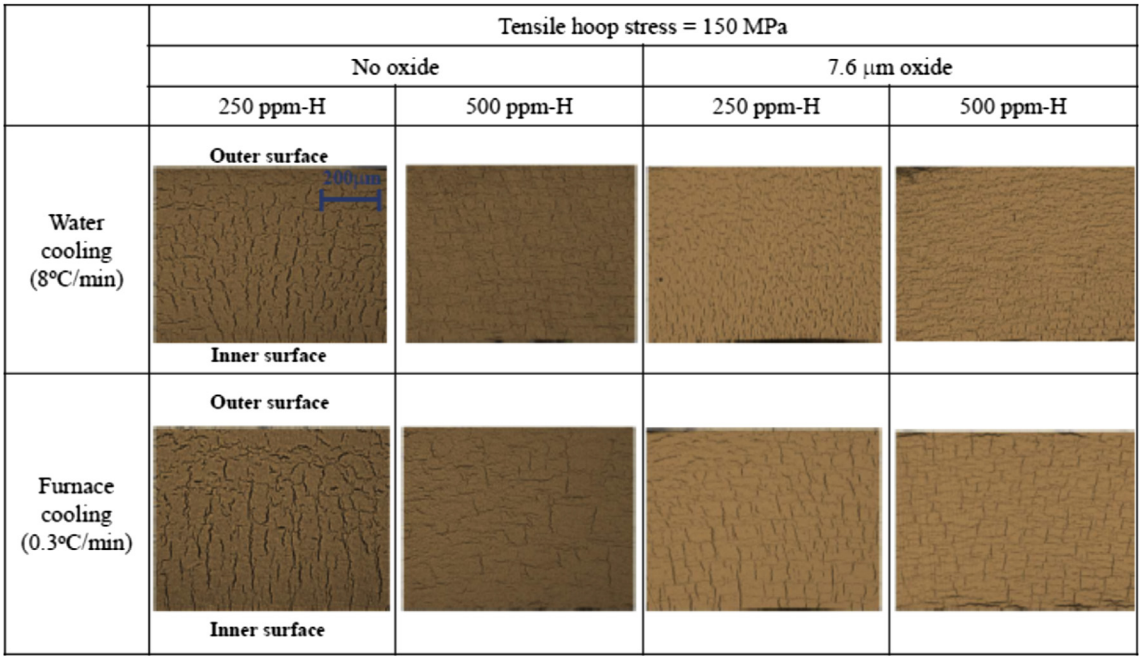

Fig. 6 – Optical micrographs of the nonoxidized and oxidized specimens cooled down to room temperature from 400°C under 150 MPa.

nucleation energy may decrease with the increase in the tensile stress. Therefore, the radial hydrides seem to be easily formed around the inner tube surface having a relatively higher hoop stress.

In order to calculate the radial hydride fraction and average length from the optical micrographs shown in Fig. 6, the circumferential and radial hydrides are to be defined as follows. The circumferential hydride is defined as the plates with an orientation within 0–40° to the circumferential axis, whereas the radial hydride have an orientation within 50–90° to the circumferential axis. The small fraction of hydrides within 40–50° to the circumferential axis was not counted as the radial or circumferential hydrides. Then, the radial hydride fractions and average lengths were determined by an image analysis program with 500× magnification optical micrographs covering all the areas of the specimens. It should be noted that only the circumferential and radial hydrides precipitated during the cool-down process were taken into account to calculate the radial hydride fractions, which is defined as the ratio of the total length of radial hydrides to the total length of circumferential and radial hydrides precipitated during the cool-down process. This means that the undissolved circumferential hydrides at 400°C for the 500 ppm-H specimens were eliminated from the total circumferential hydrides.

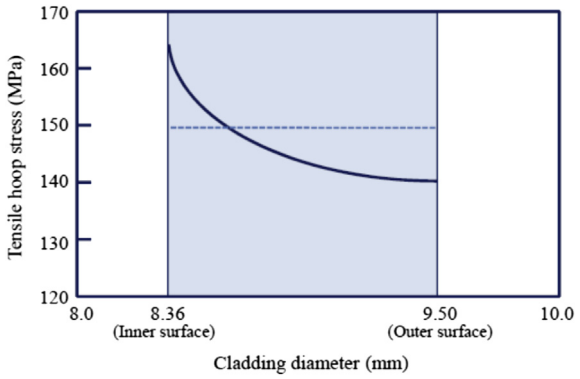

Fig. 7 – Tensile hoop stress variation in the radial direction of the cladding tube.

Based on the procedures described above, the radial hydride fractions and average lengths for the nonoxidized and oxidized specimens are given in Figs. 8 and 9, respectively. It is noteworthy that the uncertainty in the radial hydride fraction is < 5% of the average values, which was estimated from the radial hydride fractions of the six portions of the respective optical micrographs shown in Fig. 6, while the uncertainty in the radial hydride average length is within ± 2 μm, The circumferential hydride length prior to the cool-down is larger after the cool-down. The circumferential hydrides generated during the cool-down may become shorter in length with an increase in the cooling rate, just like the radial hydride lengths given in Fig. 9.

From the data shown in Figs. 8 and 9, three outstanding phenomena may be pointed out: Firstly, the slower cooling rate generated the larger radial hydride fractions and the longer radial hydride lengths. Secondly, the 250 ppm-H specimens generated larger radial hydride fractions and longer radial hydrides than the 500 ppm-H specimens. Finally, the oxidized specimens generated the smaller radial hydride fractions and the shorter hydride lengths especially for the 250 ppm-H specimens.

The amount of hydrides precipitated during the cool-down from 400°C to RT rather depends on the terminal solid

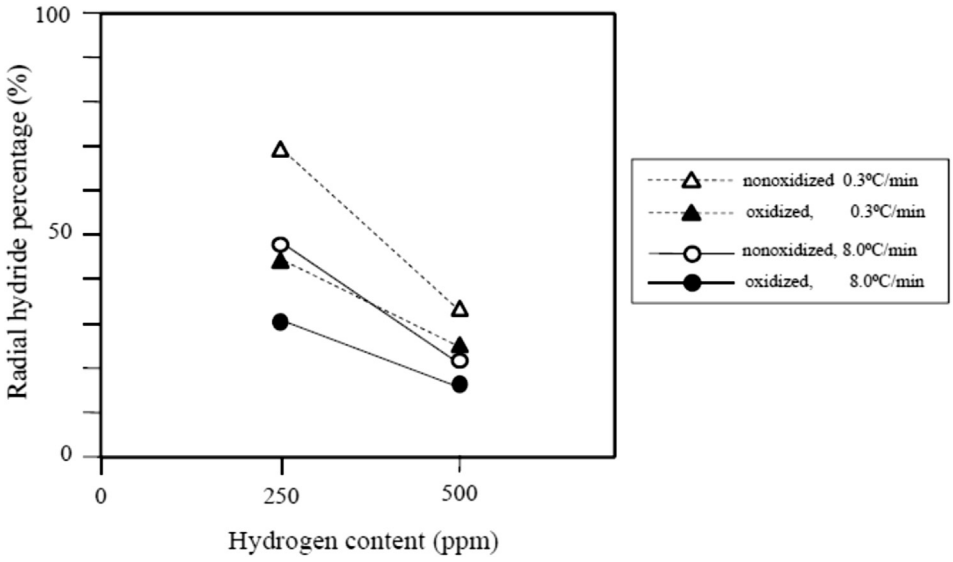

Fig. 8 – Radial hydride percentages of the nonoxidized and oxidized specimens cooled down to room temperature from 400°C under 150 MPa.

solubility dissolution curve, but the terminal solid solubility precipitation curve provides the temperature at which incipient precipitation will start during the cool down (see the dotted curve in Fig. 5). When the specimen starts to cool down from 400°C to RT, the dissolved hydrogen atoms at 400°C do not form hydrides until about 340°C because the solubility line moves along the line A–B and then the hydrogen solubility decreases along the dotted curve along the line B–C. It should be noted that the hydrogen solubilities for precipitation at 400°C and RT are about 230 ppm and 10 ppm, respectively. The comparison of these two hydrogen solubilities indicates that the dissolved hydrogen atoms of 220 ppm are to be precipitated when cooled down to RT.

The first phenomenon that the slower cooling rate generated the larger radial hydride fraction may be explained by a residence time at a relatively higher temperature during the cool-down. The dissolved hydrogen atoms of about 220 ppm at 400°C may be precipitated during the cool-down to RT in the radial and circumferential directions depending not only on their respective magnitudes of hydride nucleation energies but also on their nearest available sites of hydride nucleation. The slower cooling rate that generates a relatively long residence at a relatively high temperature may help the hydrogen atoms more easily search out the radial hydride nucleation sites with lower nucleation energies, while the faster cooling rate may compel the hydrogen atoms to diffuse to the nearest hydride nucleation sites, even with a higher nucleation energy, rather than to search out the radial hydride nucleation sites having lower nucleation energies. Therefore, the relatively longer residence time at higher temperatures may

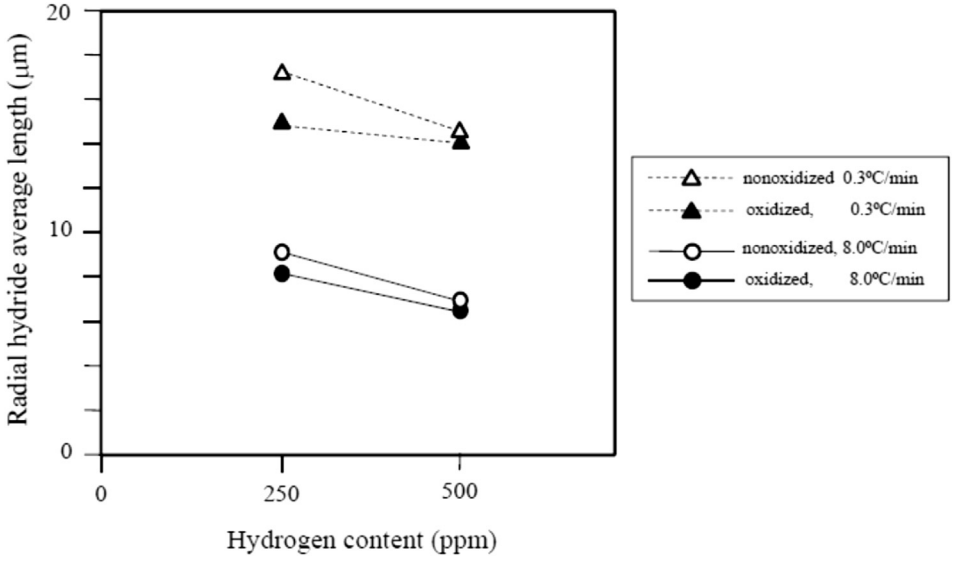

Fig. 9 – Radial hydride average lengths of the nonoxidized and oxidized specimens cooled down to room temperature from 400°C under 150 MPa.

result in the larger radial hydride fraction with the slower cooling rate, as shown in Fig. 8.

By contrast, the cooling rate-dependent hydride length variation may be explained by hydrogen supersaturation or tiny hydride particulates precipitated during the cool-down that could not be detected directly by the optical microscope and the scanning electron microscope. It is generally known that the faster cooling rate can increase the extent of hydrogen supersaturation or make precipitated particulates shorter. The indirect evidence for the hydrogen supersaturation or tiny hydride particulates may be supported by the fact that the faster cooling rate generated the shorter hydride length, as shown in Fig. 9. The change in the radial hydride length with time (Δt) may be described by the following equation developed by Puls [25], based on the Lifschitz–Slyozov–Wagner coarsening theory [26,27]:

$$a^3 - a_o^3 = \frac{16\gamma_{\alpha\delta}^2 D C_H^S \upsilon_{hyd}}{9\gamma_{\alpha\delta}^C \pi RT}\Delta t \quad (1)$$

$$D = D_o\, exp(-\Delta E/RT) \quad (2)$$

where, a_o and a are the initial and the after-growth sizes, $\gamma_{\alpha\delta}^2$ is the surface energy between hydride and zirconium matrix, $\gamma_{\alpha\delta}^C$ is the coherent surface energy between hydride and zirconium matrix, D is the diffusivity of hydrogen atoms, D_o is the pre-exponential diffusion coefficient, ΔE is the activation energy of hydrogen atom diffusion, C_H^S is the hydrogen equilibrium molar concentration, and υ_{hyd} is the molar volume of hydrogen in the zirconium matrix. Eqs. (1) and (2) indicate that each nucleated hydride will grow faster with the increase in residence time at a relatively high temperature. Considering that a residence time at a relatively high temperature increases with the slower cooling, it is natural that the slower cooling generates the longer radial hydrides than the faster cooling, as shown in Fig. 9.

The second phenomenon—that the 500 ppm-H specimens generated smaller radial hydride fractions and shorter radial hydrides than the 250 ppm-H specimens—may be explained by the relatively large amount of the undissolved circumferential hydrides of the 500 ppm-H specimens at the heat-up temperature of 400°C. The undissolved circumferential hydrides at 400°C for the 500 ppm-H specimens may play an active role in blocking up the growth of the radial hydrides and subsequently limit the radial hydride length below the distance between the adjoining circumferential hydrides. This may explain that the 500 ppm-H specimens generated the smaller fraction of radial hydrides precipitated during the cool-down and the shorter radial hydride length at the same cooling rate and the tensile hoop stress.

The third phenomenon—that the radial hydride fractions and lengths were reduced for the oxidized specimens—may be explained by oxygen-induced increase in hydrogen solubility and probably in the radial hydride nucleation energy. McMinn et al [17] reported that the hydrogen solubility increased with the oxygen-containing Zircaloy-4 materials. Yamanaka et al [18] also reported that the hydrogen solubility increased in the lower oxygen content range but decreased in the higher range. Based on these observations, it may be said that the oxidized specimens having the oxygen contents of ~2.0 w/o used in this study may have a higher hydrogen solubility at the same cool-down temperature than the nonoxidized specimens; generating the reduction in the amount of hydrogen atoms precipitated during the cool-down and subsequently smaller radial hydride fraction and shorter radial hydride length than the nonoxidized specimens. However, the reason that the oxidized specimens generated a smaller radial hydride fraction is not clear. It may be conjectured that both oxygen and hydrogen atoms may compete to occupy available radial hydride nucleation sites when a sufficient tensile hoop stress is applied. As a result, the radial hydride nucleation energy may increase due to the oxygen occupation at the radial hydride nucleation sites, causing the increase in the radial hydride nucleation energy in the oxidized specimens.

Figs. 10 and 11 show the hydrogen content-dependent ultimate tensile strengths and plastic elongations of the nonoxidized and oxidized specimens for the cooling rates of 0.3°C/min and 8.0°C/min. The ultimate tensile strengths and plastic elongations were determined using tensile hoop stress-strain curves. The plastic elongations were calculated by subtracting the elastic strain from the total strain, as explained by Kim et al [7]. As seen in Fig. 10, the as-received specimens having a hydrogen content of ~10 ppm generated nearly the same ultimate tensile stresses and plastic elongations, regardless of the cooling rates. This may be explained by the small hydrogen content of 10 ppm in the as-received specimens and by the hydrogen solubility of ~20 ppm at 100°C (see Fig. 5), indicating that hydrides in the as-received specimens may start to precipitate at temperatures below 100°C and then such hydrides, if any, may be oriented in the circumferential direction during the cool-down process since the threshold tensile hoop stress below 100°C seems to be much larger than the tensile hoop stress of 150 MPa employed in this study.

As expected, the ultimate tensile stresses and plastic elongations of the hydrogen-charged specimens were reduced drastically when the cooling rate was reduced from 8.0°C/min to 0.3°C/min, as seen in Figs. 10 and 11. As seen in Fig. 10, the nonoxidized specimens generated a higher ultimate tensile strength than the oxidized specimens, except for the nonoxidized 250 ppm-H specimen, which produced the least ultimate tensile strength. The plastic elongations of the 250 ppm-H and 500 ppm-H specimens were calculated to be zero for the cooling rate of 0.3°C/min, regardless of oxygen content in the specimens, and that of the nonoxidized 250 ppm-H specimen was calculated to be zero for the cooling rate of 8.0°C/min, as seen in Fig. 11. These mechanical degradations may be correlated with the radial hydride fractions and lengths, as shown in Figs. 8 and 9, as well as the oxygen content in the specimens.

In general, the hydride-induced mechanical degradations can be related to the hydride orientation with respect to the applied stress state. Bourcier and Koss [28] and Fan and Koss [29] indicated that for specimens with circumferential hydrides under the tensile hoop stress state, the fracture is basically ductile. The reason for this may be attributed to the fact that the shape of hydrides is approximated as a flat oblate spheroid [30–32], and the transverse fracture of the circumferential hydrides produces a much smaller fractured

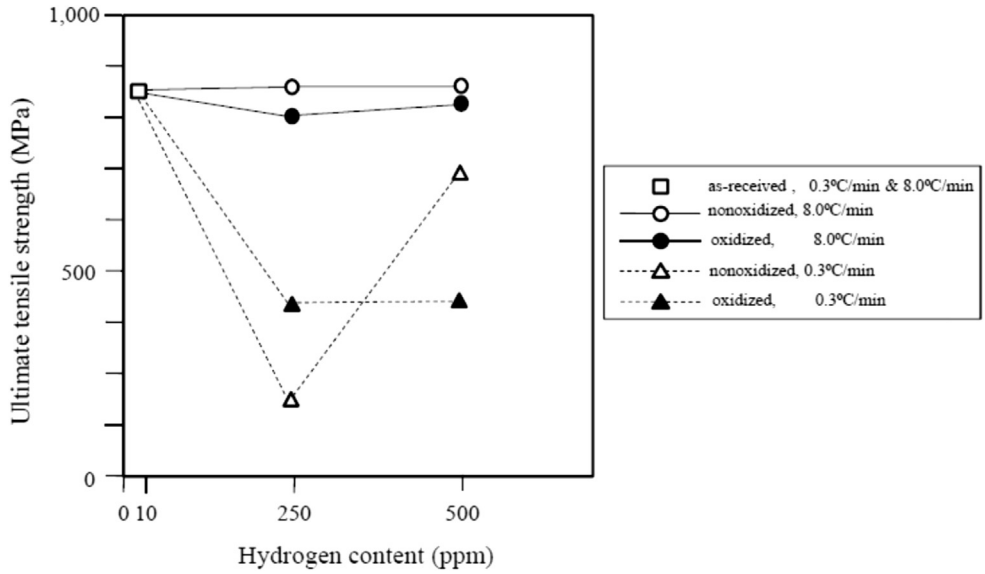

Fig. 10 – Ultimate tensile strengths of the nonoxidized and oxidized specimens cooled down to room temperature from 400°C under 150 MPa.

area than the lengthwise fracture of the radial hydrides under the tensile hoop stress state. Therefore, the radial hydrides are much more deleterious to zirconium-base alloy cladding tubes than the circumferential hydrides, especially when the radial hydrides are longer. This is because longer radial hydrides may generate an interlinked radial hydride configuration easily, which is finally transformed into through-wall fracture. As seen in Figs. 10 and 11, however, the oxidized specimens generated lower ultimate tensile strengths, except for the nonoxidized 250 ppm-H specimen, and the oxidized specimens generated much larger plastic elongations than the nonoxidized ones for the cooling rate of 8.0°C/min. This indicates that the oxygen content as well as the radial hydride fraction may compete for reducing the ultimate tensile strength and plastic elongation.

4. Conclusion

The effect of hydrogen content, oxygen content and cooling rate on radial hydride precipitation behaviors during the cool-down from 400°C to RT was investigated using as-received Zr-Nb cladding tubes and hydrogen-charged tubes with and

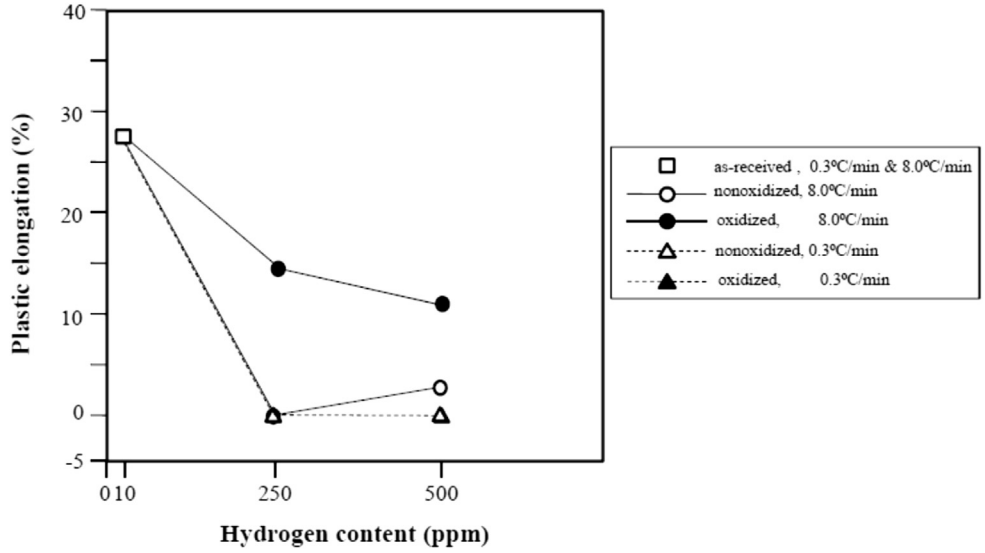

Fig. 11 – Plastic elongations of the nonoxidized and oxidized specimens cooled down to room temperature from 400°C under 150MPa.

without oxygen content. The key results obtained in this study may be given as follows:

- The slow cooling rate generated the larger radial hydride fraction. This may be explained by a residence time at a relatively higher temperature during the cool-down. As long as the applied hoop stress is larger than a certain threshold hoop stress, the slow cooling rate generating the longer residence at a relatively high temperature may help the hydrogen atoms search out radial hydride nucleation sites more easily, resulting in the larger radial hydride fraction.
- The fast cooling rate generated the shorter hydride length since hydrogen supersaturation or tiny hydride particulates that precipitate become more probable with the faster cooling rate. In addition, each nucleated hydride occurring for the slow cooling rate will grow faster with the increase in the residence time at a relatively high temperature.
- The 250 ppm-H specimens generated larger radial hydride fractions, longer radial hydrides, and smaller ultimate tensile strengths and plastic elongations than the 500 ppm-H specimens. This may be explained by the relatively larger amount of the undissolved circumferential hydrides and the smaller amount of the radial hydrides of the 500 ppm-H specimens at the heat-up temperature of 400°C. The remaining circumferential hydrides at 400°C might block the growth of the radial hydrides and subsequently limit the radial hydride length below the distance between the adjoining circumferential hydrides.
- The oxidized specimens generated a smaller radial hydride fraction and shorter hydride length than the nonoxidized specimens. This may be explained by an oxygen-induced increase in the hydrogen solubility.
- Ultimate tensile strength and plastic elongation can be correlated with oxygen content as well as radial hydride fraction. In general, the oxidized specimens generated lower ultimate strength and plastic elongation than the nonoxidized only if the radial hydride fraction is relatively small, indicating that the oxygen content as well as the radial hydride fraction may compete for reducing the ultimate tensile strength and plastic elongation.

Conflicts of interest

All authors have no conflicts of interest to declare.

Acknowledgments

This research was supported by the Dongguk University Research Fund of 2015; and by the Nuclear Energy Development Program (No. 2014M2A8A5021211 and No. 2013M2A8A1060018) through the National Research Foundation of Korea (NRF) funded by the Ministry of Science, ICT and Future Planning as well as by the project titled, Evaluation of Database for Mechanical, Corrosion and Fretting Wear Characteristics of Inconel 690 Straight Tubes, funded by the Ministry of Trade, Industry & Energy.

REFERENCES

[1] R. Singh, R. Kishore, S. Singh, T. Sinha, B. Kashyap, Stress-reorientation of hydrides and hydride embrittlement of Zr–2.5 wt% Nb pressure tube alloy, J. Nucl. Mater. 325 (2004) 26–33.
[2] H. Chung, Understanding hydride- and hydrogen-related processes in high-burnup cladding in spent-fuel storage and accident situations, in: Proceedings of the International Topical Meeting on Light Water Reactor Fuel Performance, Orlando (FL), 2004, p. 470.
[3] J. Won, M. Kim, K. Kim, Heat-up and cool-down temperature-dependent hydride reorientation behaviors in zirconium alloy cladding tubes, Nucl. Eng. Tech. 46 (2014) 681–688.
[4] J. Won, S. Min, K. Kim, Cooldown-induced hydride reorientation of hydrogen-charged zirconium alloy cladding tubes, Met. Mat. Int. 21 (2015) 31–42.
[5] S. Min, J. Won, K. Kim, Terminal cool-down temperature-dependent hydride reorientations in Zr–Nb alloy claddings under dry storage conditions, J. Nucl. Mater. 448 (2014) 172–183.
[6] S. Min, M. Kim, K. Kim, Cooling rate- and hydrogen content-dependent hydride reorientation and mechanical property degradation of Zr–Nb alloy claddings, J. Nucl. Mater. 441 (2013) 306–314.
[7] M. Kim, H. Kim, S. Min, K. Kim, Cladding cooling rate-dependent hydride reorientation and configuration, Korean J. Met. Mater. 51 (2013) 477–486.
[8] S. Min, M. Kim, C. Won, K. Kim, Effects of cooling rates on hydride reorientation and mechanical properties of zirconium alloy claddings under interim dry storage conditions, Korean J. Met. Mater. 51 (2013) 487–495.
[9] R. Marshall, M. Louthan Jr., Tensile properties of Zircaloy with oriented hydrides, Trans. ASM 56 (1963) 693–700.
[10] M. Louthan Jr., R. Marshall, Control of hydride orientation in Zircaloy, J. Nucl. Mater. 9 (1963) 170–184.
[11] S. Hong, K. Lee, Stress-induced reorientation of hydrides and mechanical properties of Zircaloy-4 cladding tubes, J. Nucl. Mater. 340 (2005) 203–208.
[12] P. Bouffioux, A. Ambard, A. Miquet, C. Cappelaere, Q. Auzoux, M. Bono, O. Rabouille, S. Allegre, V. Chabretout, C.P. Scott, Hydride Reorientation in M5 Cladding and its Impact on Mechanical Properties, Top Fuel 2013, Charlotte (NC), 2013, p. 879.
[13] R. Marshall, Influence of fabrication history on stress-oriented hydrides in Zircaloy tubing, J. Nucl. Mater. 24 (1967) 34–48.
[14] R. Marshall, Control of hydride orientation in Zircaloy by fabrication practice, J. Nucl. Mater. 24 (1967) 49–59.
[15] J. Kearns, C. Woods, Effect of texture, grain size, and cold work on the precipitation of oriented hydrides in Zircaloy tubing and plate, J. Nucl. Mater. 20 (1966) 241–261.
[16] M. Leger, A. Donner, The effect of stress on orientation of hydrides in zirconium alloy pressure tube materials, Can. Metall. Q. 24 (1985) 235–243.
[17] A. McMinn, E. Darby, J. Schofield, The terminal solid solubility of hydrogen in zirconium alloys, in: 12th International Symposium on Zirconium in the Nuclear Industry, Toronto, Canada, 2000, p. 173.
[18] S. Yamanaka, Y. Fujita, M. Uno, M. Katsura, Influence of interstitial oxygen on hydrogen solubility in metals, J. Alloys Compounds 293 (1999) 42–51.
[19] H. Kim, Y. Jeong, K. Kim, The effects of creep and hydride on spent fuel integrity during interim dry storage, Nucl. Eng. Tech. 42 (2010) 249–258.
[20] H. Kim, I. Kim, S. Park, J. Park, Y. Jeong, Evaluation of hydride effect on fuel cladding degradation, Kor. J. Met. Mater. 48 (2010) 717–723.

[21] K. Colas, A. Motta, J. Almer, M. Daymond, M. Kerr, A. Banchik, *In situ* study of hydride precipitation kinetics and re-orientation in Zircaloy using synchrotron radiation, Acta Mater. 58 (2010) 6575–6583.
[22] W. Qin, J. Szpunar, J. Kozinski, J. Kozinski, Hydride-induced degradation of hoop ductility in textured zirconium-alloy tubes: a theoretical analysis,, Acta Mater. 60 (2012) 4845–4855.
[23] H. Chung, Fundamental metallurgical aspects of axial splitting in Zircaloy cladding, in: Proceedings of the International Topical Meeting on Light Water Reactor Fuel Performance, Park City (UT), 2000, p. 325.
[24] P. Vizcaíno, P.B. Bozzano, A.V. Flores, A.D. Banchik, R.A. Versaci, R.O. Ríos, Hydrogen solubility and microstructural changes in Zircaloy-4 due to neutron irradiation, J. ASTM Int. 8 (2011) 1–20.
[25] M. Puls, Hydrogen-induced Delayed Cracking: 2. Effects of Stress on Nucleation, Growth and Coarsening of Zirconium Hydride Precipitates, AECL-8381, Atomic Energy of Canada, Whiteshell Nuclear Research Establishment, Pinawa, Manitoba (Canada), 1984.
[26] I. Lifshitz, V. Slyozov, Kinetics of diffuse decomposition of supersaturated solid solutions, Soviet Phys. JETP 35 (1959) 331–339.
[27] C. Wagner, Theorie der alterung von niederschlagen durch umlosen (Ostwald-Reifung), Z. Elektrochem 65 (1961) 581–591 [In German].
[28] R. Bourcier, D. Koss, Hydrogen embrittlement of titanium sheet under multiaxial states of stress, Acta Metall. 32 (1984) 2091–2099.
[29] Y. Fan, D. Koss, The Influence of multiaxial states of stress on the hydrogen embrittlement of Zr alloy sheet, Metall. Trans. A 16 (1985) 675–681.
[30] D. Northwood, U. Kosasih, Hydrides and delayed hydrogen cracking in zirconium and its alloys, Int. Met. Rev. 28 (1983) 92–121.
[31] G. Itoh, M. Kanno, T. Hagiwara, T. Sakamoto, Embrittlement in an age-hardened 2091 aluminum alloy by exposure at elevated temperatures below the aging temperature, Acta Mater. 47 (3799) (1999) 3799–3809.
[32] V. Perovic, G. Weatherly, C. Simpson, Hydride precipitation in α/β zirconium alloys, Acta Metall. 31 (1983) 1381–1391.